European Journal of Radiology 142 (2021) 109832

Contents lists available at ScienceDirect

European Journal of Radiology

journal homepage: www.elsevier.com/locate/ejrad

Possibility to discriminate benign from malignant breast lesions detected on dual-layer spectral CT-evaluation

Begüm Demirler Şimşir [a,b,1], Kathrin Barbara Krug [c,1,*], Christina Burke [c], Martin Hellmich [d], David Maintz [c], Emmanuel Coche [a]

[a] Department of Radiology, Cliniques Universitaires St-Luc, Université Catholique de Louvain, Brussels, Belgium
[b] Department of Radiology, University of Health Sciences, Dışkapı Yıldırım Beyazıt Training and Research Hospital, Ankara, Turkey
[c] Department of Diagnostic and Interventional Radiology, University Hospital of Cologne, Germany
[d] Institute of Medical Statistics and Bioinformatics, University of Cologne, Germany

ARTICLE INFO

Keywords:
Computed tomography (CT)
Breast imaging
Multiparametric CT
Quantitative CT
Breast cancer

ABSTRACT

Objectives: Intramammary mass lesions are reportedly present in up to 5.8% of all contrast enhanced CT-examinations of the female chest. We aimed to assess whether their biological relevance can be estimated using spectral CT-datasets.

Methods: In this bicentric retrospective study patients with breast masses visualized on spectral CT-examinations from 07/2017 to 06/2019 were included. Lesions were characterized as malignant or benign based on histology and/or a stable follow-up of >2 years. Conventional CT-images, iodine density-maps, virtual monoenergetic-images (40 keV, 100 keV) and Zeffective-maps were evaluated by two independent readers. Statistical analysis derived from the Regions of interest (ROIs) was done by calculating the Areas under the Receiver operating characteristic (ROC) curve (AUC) and Youden-indices.

Results: 106 breast masses (malignant/benign: 81/25, 76.4%/23.6%) were included. The mean AUCs of the variables "iodine content" (reader 1/2:0.97;0.98), "monoenergetic curve-slope" (0.97;0.96) and "Zeffective" (0.98;0.98) measured in the target lesions (TL) showed superior results compared to those derived from the variable "density" (0.92;0.93) ($p < 0.001$). The ratios "TL to aorta" calculated for the variables "iodine content", "monoenergetic curve-slope" and "Zeffective" showed superior results compared to normal breast tissue and muscle ($p < 0.001$). The optimal cutpoint for the "iodine content" in the TL was 0.7–0.9 mg/ml (sensitivity 96.6%, specificity 91.7%). The best diagnostic results were achieved by normalizing the iodine content in the TL to that in the aorta (optimal cutpoint 0.1, sensitivity 95.5%, 98.9%, specificity 91.7%).

Conclusions: Our preliminary results suggest that spectral CT-datasets might allow to estimate the biological dignity of breast masses detected on clinically indicated chest-examinations.

1. Introduction

Although computed tomography (CT) is not a modality for evaluation of breast masses, it has been previously reported that incidental breast masses needing diagnostical clarification are detected in up to 5.8% of all contrast-enhanced conventional CT-examinations ot the female chest [1–5]. Comparable to breast MRI, the breast imaging findings related to malignancy in conventional CT have been documented as spiculated or irregular margins and irregular shape [2,3,6]. Rim or heterogeneous enhancement could suggest malignancy, however, without dynamic examination, this feature does not provide sufficient information for differentiation. Spectral-CT is being increasingly used since 2006 and has been shown to add value in oncological imaging in several organ systems [7–9]. By acquiring attenuation values at two different energy levels, additional datasets can be generated such as virtual monoenergetic (VM) and material decomposition maps in

Abbreviations: AUC, Area under the curve; CT, Computed tomography; HU, Hounsfield unit; J, Youden index; R, Reader; ROC, Receiver operating characteristic curves; ROI, Region of interest; TL, Target lesion; VM, Virtual monoenergetic; Zeff., Z effective.

* Corresponding author at: Dept. of Diagnostical and Interventional Radiology, University Hospital of Cologne, 50924 Cologne, Germany.
E-mail address: Barbara.krug@uk-koeln.de (K.B. Krug).

[1] shared first authorship.

https://doi.org/10.1016/j.ejrad.2021.109832
Received 27 April 2021; Received in revised form 10 June 2021; Accepted 21 June 2021
Available online 24 June 2021

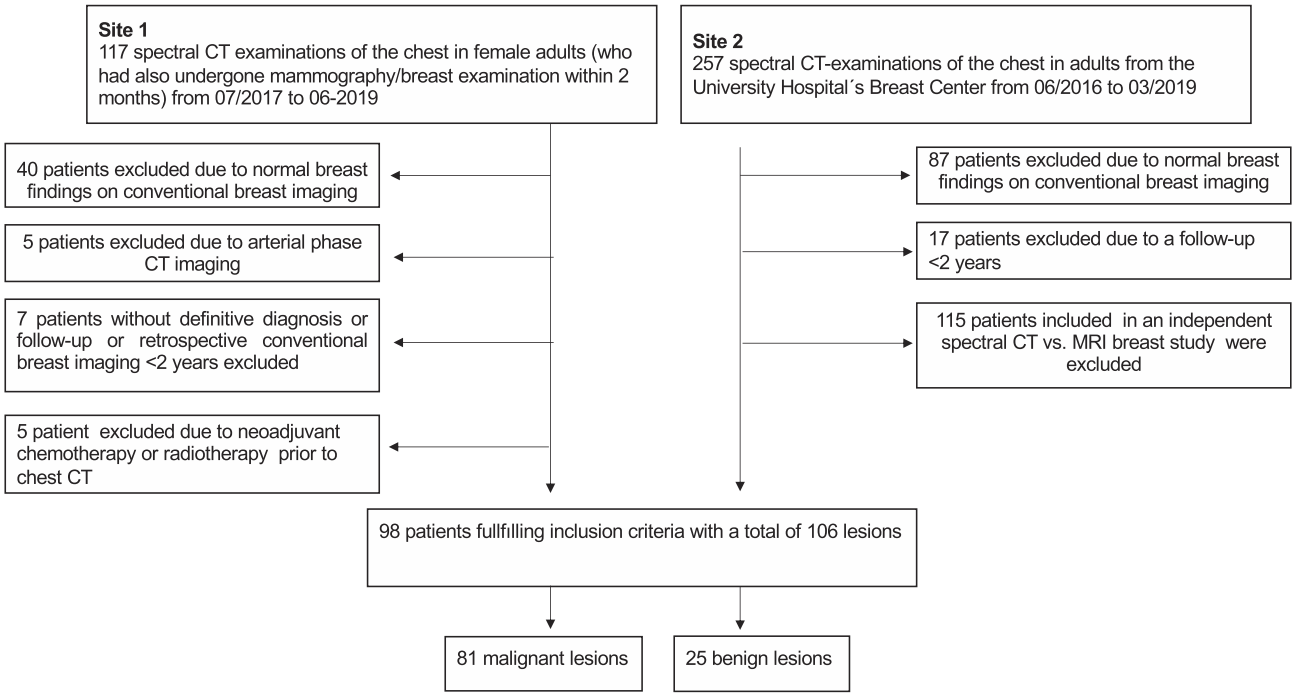

Fig. 1. Recruitment of patients from the databases at both sites.

addition to conventional images [11–13]. Iodine density-maps provide quantitative information about tissue vascularity and perfusion. VM-images at lower keV allow enhancement of iodine and could lead to a better delineation of breast lesions that contain iodine thus increasing their visibility and detectability [9,10]. Color-coded Zeffective-images discriminate different tissues based on their effective atomic number which has been demonstrated as superior to HU-comparison on conventional CT [7–10]. Regardless of the technical approach of the spectral-CT vendors, VM and material decomposition images could be obtained [11–14]. Dual-layer CT imaging is characterized by the fact that the radiation spectrum received by the detector is automatically registered in the form of 2 energetically different energy spectra without changing the tube voltage and tube current intensity used for the examination, i.e. with an unchanged exposure dose compared to conventional CT, so that all CT-examinations performed with a dual-layer detector can be retrospectively evaluated in dual-spectral technique [9–11,14]. This feature obviates the need for a prior selection of a protocol to generate additional datasets.

There are only few studies discussing spectral-CT findings of breast lesions including up to 42 patients and their results are promising in discriminating malignant lesions [15–18]. Okamura et al. [15] assessed non-contrast and contrast-enhanced VM-images at 100, 120 and 140 keV. In both, non-contrast and contrast-enhanced images the Hounsfield values of malignant tissues were higher than those of normal breast tissue indicating the effectiveness of dual-energy CT in the diagnosis of breast cancer. Okada et al. [16] evaluated the visibility of malignant breast lesions on VM-images reconstructed stepwise from 40 to 80 keV out of 4-phasic CT-data sets and described a favorable match between image quality and iodine uptake at 50 keV. Metin and colleagues [17] confirmed that the conspicuity of breast cancer was higher in low VM-images obtained at 40 keV with breast cancer. Volterrani et al. [18] observed the optimal AUC-thresholds on VM-images obtained at 40 and 70 keV at an iodine concentration of 1.7 mg/mL.

Thus, we aimed to investigate the diagnostic value of quantitative multiparametric data such as iodine content, VM curve-slope, and Zeffective-values in predicting the oncological significance of the breast masses detected on dual-layer spectral-CT.

2. Methods and materials

2.1. Study population

This retrospective bicentric study was approved by both local institutional ethical review boards (file numbers 2019/06MAR/110 and 17-167). The patient examinations were extracted from the institutional Picture Archiving- and Communication Systems (PACS) (Carestream®, Philips Healthcare, Cleveland, Ohio, USA; ImpaxEE®, AGFA Healthcare, NV, Mortsel, Belgium).

The inclusion criteria differed slightly at site 1 and site 2 due to the fact that the study surveys were initially started independently of each other and were only combined as the study progressed. At site 1 all adult patients with breast masses visualized on a clinically indicated CT-examination who had also undergone X-ray mammography and breast ultrasound within 2 months of the CT-examination between 07/2017 and 06/2019 for staging of newly diagnosed carcinoma, restaging in case of suspicious oncological relapse or staging in case of unknown primaries were included (Fig. 1). At site 2 all adult patients who underwent a spectral-CT scheduled by the Breast Center between 06/2016 and 03/2019 indicated for staging/re-staging due to breast cancer with a histological work-up of the CT target lesions within 2 months were included in the evaluations.

The exclusion criteria were as follows: patient age < 18 years, >2 months between the CT-examination and mammography/ultrasound, CT-data acquisition in the arterial phase after i.v. contrast administration, no follow-up or retrospective conventional breast imaging of > 2 years for probable benign masses that are not proven by histopathology, neoadjuvant chemotherapy between the CT-examination and obtaining the histological diagnosis and prior ipsilateral radiotherapy in patients with a history of breast cancer.

Breast lesions were characterized as malignant based on histopathology or benign based on histopathology and/or stability for at least two years of follow-up or retrospective conventional breast imaging assessment.

Table 1
Demographics. Two male participants of site 2 both with gynaecomastia vera and both with breast cancer stage pT1c N0 M0 and cT4c cN1 cM1, respectively. SD = standard deviation.

Parameter	Site 1	Site 2	Both sites
Total no. of participants (**N**; %)	**60**; 61.2	**38**; 38.8	**98**; 100.0
Total no. of lesions (**N**; %)	**66**; 62.3	**40**; 37.7	**106**; 100.0
Female participants (**N**; %)	**60**; 100.0	**36**; 94.4	**96**; 98.0
Patient age; mean, range (y)	**58.8**; 26–91	**59**; 34–84	**58.9**; 26–91
Ultrasound-guided biopsies (**N**; %)	**47;** 71.2	**33**; 82.5	**80;** 75.5
Ultrasound-guided aspiration (N; %)	**1;** 1.5	**0**	**1;** 0.9
Punch biopsies (**N**; %)	**0**	**2**; 5.0	**2;** 1.9
X ray-guided vacuum assisted biopsies (**N**; %)	**0**	**2**; 5.0	**2;** 1.9
Explorative surgery (N; %)	**0**	**3**; 7.5	**3;** 2.8
Follow-up ≥ 2 years (N; %)	**18;** 27.3	0	**18;** 17.0
Ratio of malignant-to-benign findings (**N**; %)	**42 to 24**; (57.1 to 42,9)	**39 to 1**; 97.5 to 2.5	**81 to 25**; 23.6 to 76.4
Invasive ductal carcinoma (**N**; %)	**33;** 50	**30**; 75.0	**63**; 59.4
Invasive lobular carcinoma (**N**; %)	**5;** 7.5	**4**; 10.0	**9;** 8.5
Invasive carcinoma of other types (**N**; %)	**2;** 3.0	**3**; 7.5	**5;** 4.5
Lymph node metastasis (**N**; %)	**0**	**1**; 2.5	**1;** 0.9
Benign mass lesions (N; %)	**18;** 27.5	**1;** 2.5	**19;** 20.9
Scar tissue	**6**; 9	**0**	**6;** 5.8
T1 N0 (**N**; %)	**1;** 2.4	**1;** 2.8	**2;** 2.6
T1mi/is N0 (**N**; %)	**2;** 4.8	**0;** 0.0	**2**; 2.6
T1a N0 (**N**; %)	**0;** 0.0	**1;** 2.8	**1;** 1.3
T1b N0 (**N**; %)	**0;** 0.0	**7;** 19.7	**7;** 9.1
T1c N0 (**N**; %)	**9;** 22.0	**5;** 13.8	**14;** 18.2
T1 N1 (**N**; %)	**1;** 2.4	**0;** 0.0	**1**; 1.3
T1c N1-2 (**N**; %)	**2;** 4.8	**5;** 13.8	**7;** 9.1
T1c Nx (**N**; %)	**1;** 2.4	**1;** 2.8	**2;** 2.6
T2 N0 (**N**; %)	**7;** 17.2	**8;** 22.2	**15;** 19.5
T2 N1-3 (**N**; %)	**11;** 26.9	**5;** 13.8	**16;** 20.7
T3 N0 (**N**; %)	**1;** 2.4	**0;** 0.0	**1;** 1.3
T3 N1-3 (**N**; %)	**4;** 9.9	**0;** 0.0	**4;** 5.2
T3 Nx (**N**; %)	**1;** 2.4	**0;** 0.0	**1;** 1.3
T4 N1-2 (**N**; %)	**1;** 2.4	**3;** 8.3	**4**; 5.2

2.2. CT-examination technique and data reconstruction

All CT-data were acquired on 128-row spectral detector CT scanners (Iqon®, Philips Healthcare, Cleveland, Ohio, USA) using the following routine clinical scanning parameters without specific optimization: slice collimation = 128 × 0.625 mm, pitch 1.11 (site 1) and 0.671 (site 2), slice thickness 3 and 2 mm, increment 3 and 1 mm, rotation time 0.4 and 0.3 s, tube potential 120 kVp, tube current–time product 125 mAs, dose modulation, i.v. administration of 100 ml of a nonionic iodinated contrast-medium (Xenetix® 350 mg/ml, Guerbet, Aulnay-sous-bois, France; Accupaque® 350 mg/mL, GE Healthcare, UK) at a flow rate of 2.5 to 4.0 ml/sec with a contrast bolus-delay of 70 sec followed by 30 ml of saline flush.

The reconstructed field of view was individually adjusted using a pixel-matrix of 512 × 512. From the acquired raw-data, images were reconstructed using a slice thickness of 3 mm (site 1) and 2.0 mm (site 2) and an increment of 0.0 mm with a hybrid iterative reconstruction algorithm (iDose®, Philips Healthcare, Cleveland, Ohio, USA) using the iteration level 4 and a dedicated cardiac stent convolution kernel (XCD). All quantitative analyses were performed with a fixed window width of 300 HU and a window center of 60 HU.

Spectral image-datasets were acquired by dual-layer detector-technology contained information on energy-dependent absorption thus allowing the generation of material decomposition images and VM-images with dedicated software in addition to the calculation of conventionally processed CT images. Reconstruction of conventional images, iodine density and Zeffective-maps and VM-image analysis were performed automatically on a dedicated vendor console and software platform using the same spectral raw data sets (IntelliSpace®, Philips Healthcare, Cleveland, Ohio, USA).

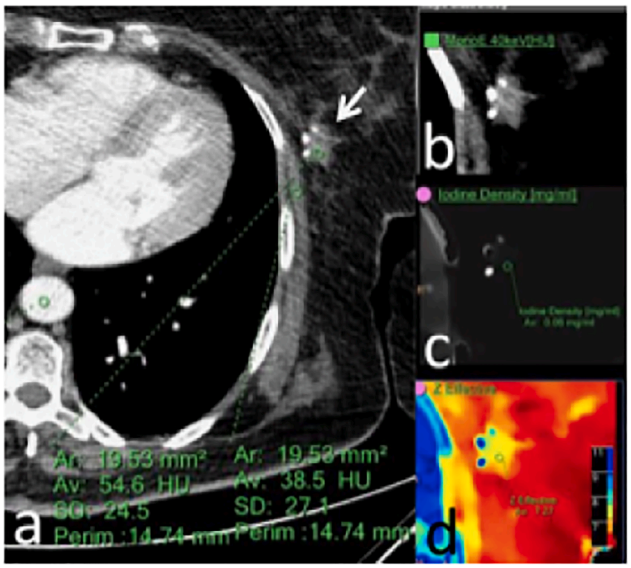

Fig. 2. 68 year-old female, follow-up imaging of the patient with a history of invasive atypical lobular carcinoma of the left breast who had been treated conservatively in 2005. (a) Scar tissue with irregular margins in the lower lateral quadrant with a density of 54.6 HU on the conventionally displayed CT-images (arrow). (b) Lower keV (40 keV) VM images show no significant attenuation difference indicating contrast uptake in scar tissue. (c) İodine density-map demonstrates lack of iodine in scar tissue (0.06 mg/ml). (d) Zeffective-map shows low atomic number of the scar tissue (7.27) without iodine content. The appearance of the scar tissue was stable between 8/2016 and 3/2019 on X-ray mammography.

2.3. Image analysis

Conventional CT-images, iodine density-maps, VM-images at 40 and 100 keV and Zeffective-maps were automatically calculated from the spectral-CT raw data sets of each examination. Image data were pseudonymized and stored as uncompressed DICOM-files in the PACS-devices. All CT-images were evaluated by two board certified radiologists with 7 (BD) and 25 years (BK) experience in breast and CT-imaging independently from each other. The readers who were blinded to the patients history and final diagnoses interactively marked circular regions of interest (ROI) in the breast target lesion as well as in normal glandular breast tissue, in muscle tissue and in the thoracic aorta or in the subclavian artery if the target lesion was located in the supraaortic upper quadrants of the breast always using the same CT tomogram. Then the ROIs were copied semi-automatically onto the iodine density-maps, the Zeffective-maps and the virtual monoenergetic-images. ROIs were drawn as large as possible to encompass most of the solid/enhancing part of the masses. Special care was taken to avoid necrotic, cystic and calcified areas in masses with mixed character. HU-values of the lesions on conventional CT-images, 40 and 100 keV virtual monoenergetic images and iodine concentrations on iodine-maps were measured with a circular ROI (reader 1: mean area 30.4 mm^2, range 0.7–131.9 mm^2, reader 2: 32.6 mm^2, 3.1–218.0 mm^2). All ROIs were placed on the axial CT-slice of the breast lesion in order to minimize variations in density and iodine concentration caused by the physiological circulatory condition of the patients. In patients with multiple lesions of similar characteristics, the two most contrast-enhancing lesions were evaluated. The

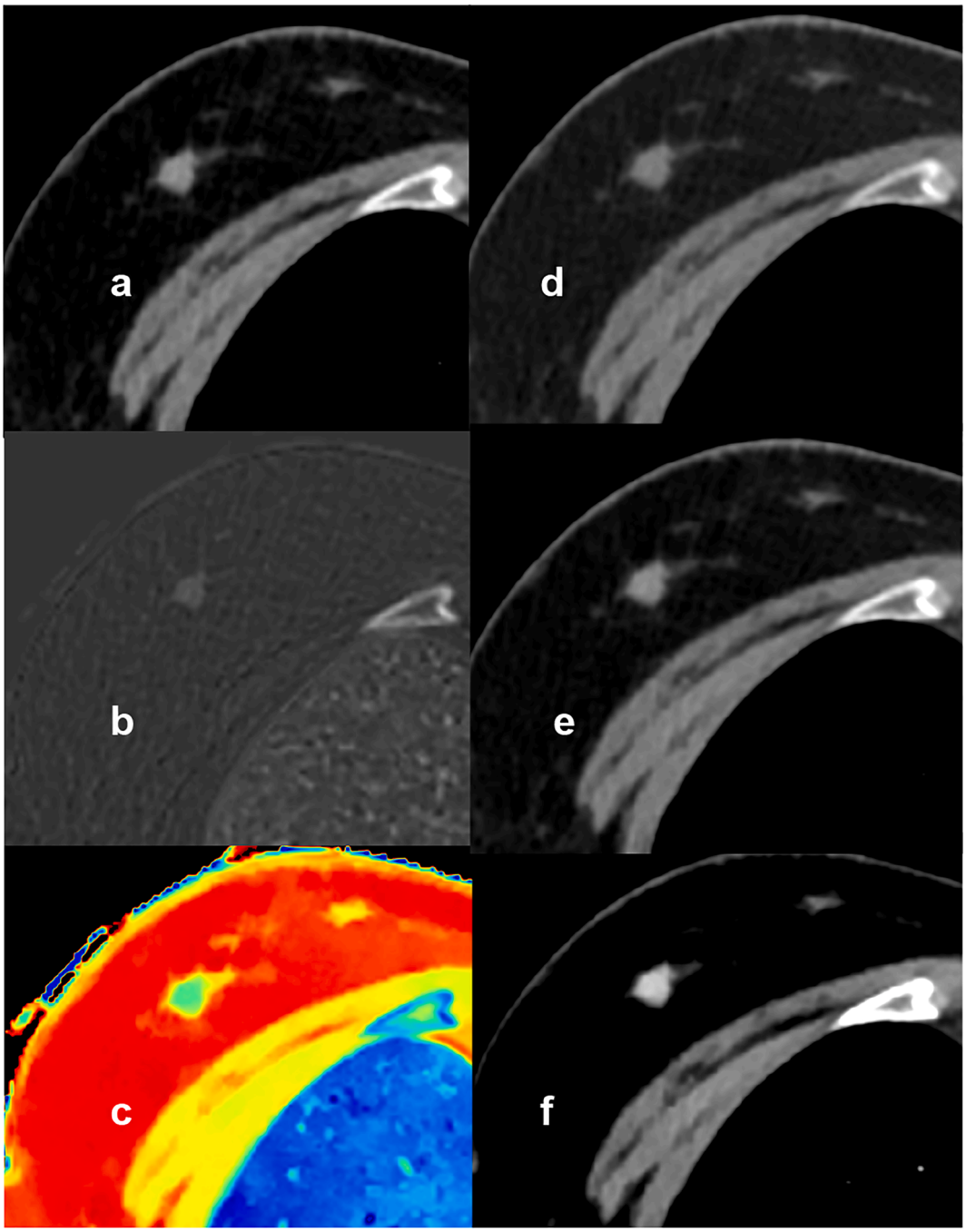

Fig. 3. 46-year-old female patient with recurrent invasive ductal breast cancer, G3, triple negative, Ki-67 90%, of 5 mm diameter on the surgical resectate. Solid tumor with irregular margins and a mean density of 83.6 HU on the conventional CT-image (a), an iodine-uptake of 1.39 mg/ml in the iodine-map (b), an elevated Z effective value of 8.10 on the Zeffective-map (c) and increasing mean densities in the virtual monoenergetic images from 57.9 HU at 100 keV (d), over 78.11 HU at 70 keV (e) to 161.8 HU at 40 keV (f).

size and shape of the ROIs were kept constant for each patient by using the "copy and paste" function of the workstation.

2.4. Statistical analysis

The iodine concentrations (mg/ml), Hounsfield Units (HU) and Zeffective-values (absolute numbers) derived from the CT-images and maps were digitally documented (Excel®, Microsoft Corp., Redmond, WA, USA). The statistical calculations were carried out using SPSS® Statistics (IBM Corp., Armonk, NY, USA) and Stata/SE® (StataCorp LLC, College Station, TX, USA). All variables were summarized by mean, standard deviation (SD), minimum (min) and maximum (max) values. The following primary calculations were carried out independently for both readers:

- The slope (k) of the spectral curve was calculated as the CT-attenuation difference at the energy levels 40 and 100 keV divided by the energy difference between these two energy levels (60 keV). The range was chosen due to the curve being almost flat between 100 and 140 keV in general.
- The ratios of the values measured in the target breast lesions and the corresponding values in normal breast tissue, in muscle tissue and in

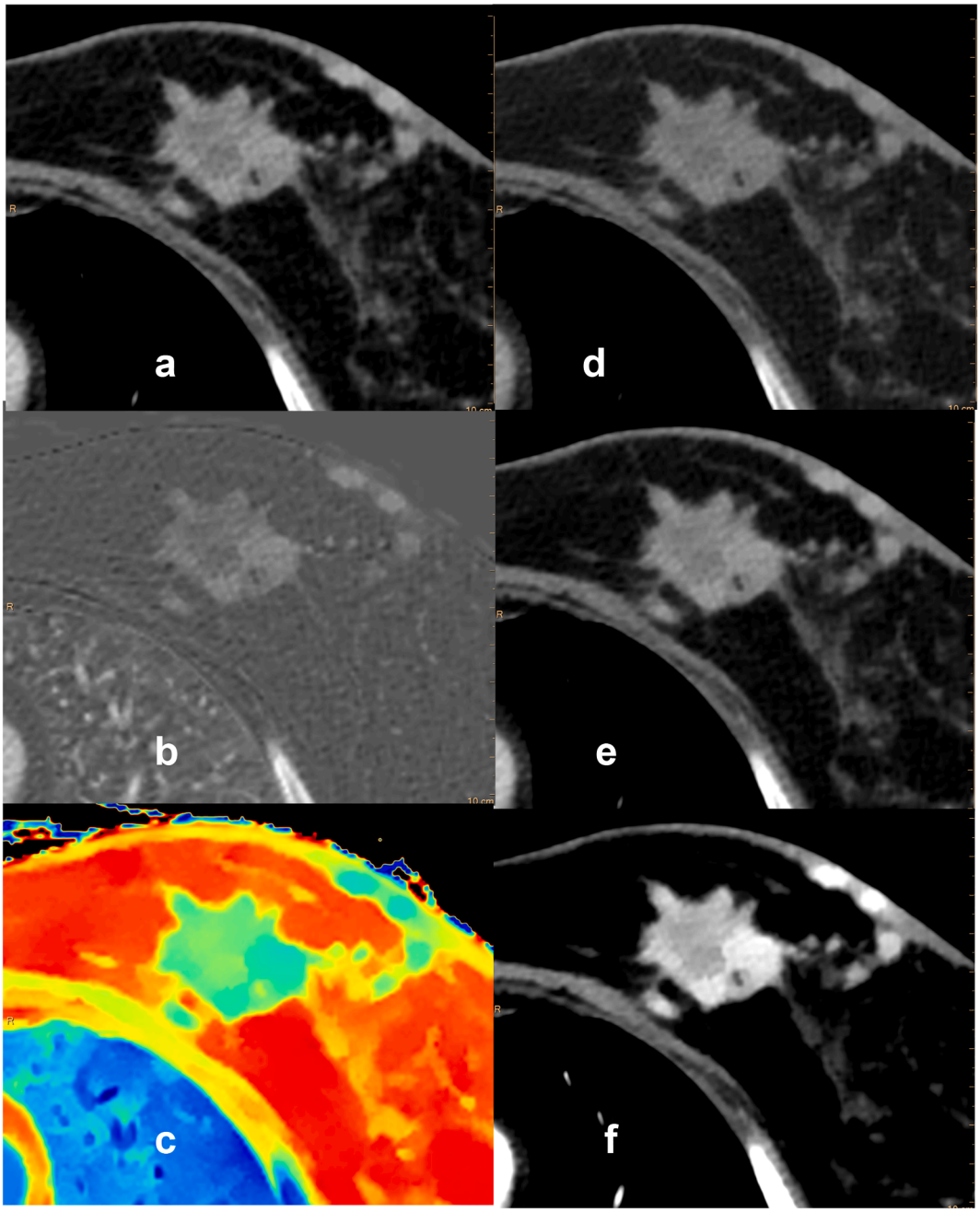

Fig. 4. 71-year-old female patient with an invasive ductal carcinoma, G2, luminal A-type, Ki-67 14%, cT4b, cN1, cM1 with lung and liver metastases proven by ultrasound-guided biopsy. (a) The conventional CT images show an inhomogeneous solid tumor of 3.7 cm maximum diameter and a mean density of 91.4 HU in its most contrast-absorbing portion. (b) The mean iodine content determined in the iodine-map was 2.18 mg/ml and (c) the mean Z-effective value was 8.45. The density values determined from the virtual monoenergetic image series are as follows: (d) 58.5 HU at 100 keV, (e) 90.03 HU at 70 keV and c) 220.3 HU at 40 keV.

the aorta were calculated in order to normalize the iodine concentration in the TL for minimizing variations caused by circulation status of the patients.

Statistical analysis was done separately for each reader using histopathology of the target lesions as reference standard. For the sake of simplicity, two histologically verified lesions per patient (8 cases) were regarded as independent entities. Receiver operating characteristic (ROC) curves were generated in order to assess the interplay of sensitivity and specificity for all test scenarios described. The diagnostic performances were determined by calculating the area under the ROC curve (AUC) with asymptotic 95%-confidence intervals. The difference in AUC from 0.5 corresponding to random classification was also assessed asymptotically, based on the calculated standard error. The Youden index (J) was used to determine the optimal cutpoint to discriminate benign from malignant findings, i.e. "J = sensitivity + specificity-1", possible J-values ranging between 0 and 1 with higher values indicating favourable results [19]. All analyses are essentially explorative with p-values $\leq$ 0.05 (*) indicating moderate evidence, p-values $\leq$ 0.01 (**) intermediate evidence and p-values $\leq$ 0.001 (***) strong evidence against the null hypothesis (e.g. zero correlation).

Table 2
Comparison of AUCs separately for each reader. The ratio of benign to malignant findings was 24 to 88 in all cases. AUC = area under the ROC curve, TL = target lesion.

Variables	Measure sites	Benign: malignant (N)	Reader 1				Reader 2			
			AUC	95% Confidence Interval		TL vs. 1), 2), 3), resp.	AUC	95% Confidence Interval		TL vs. 1), 2), 3), resp.
				Lower Bound	Upper Bound	p		Lower Bound	Upper Bound	p
Density (HU)	Target Lesion (TL)	24:88	0,929	0,873	0,985		0,923	0,871	0,976	
	1) Breast Tissue	24:80	0,581	0,463	0,699	<0.001	0,588	0,470	0,705	<0.001
	2) Muscle Tissue	24:88	0,599	0,471	0,727	<0.001	0,558	0,443	0,673	<0.001
	3) Aorta	24:88	0,346	0,201	0,491	<0.001	0,356	0,214	0,499	<0.001
Iodine content (mg/ml)	Target Lesion (TL)	24:88	0,974	0,934	1,000		0,976	0,943	1,000	
	1) Breast Tissue	24:80	0,507	0,380	0,635	<0.001	0,536	0,409	0,664	<0.001
	2) Muscle Tissue	24:88	0,481	0,358	0,603	<0.001	0,563	0,446	0,679	<0.001
	3) Aorta	24:88	0,317	0,176	0,457	<0.001	0,321	0,181	0,462	<0.001
Monoenergetic curve slope (HU 40 keV – HU 100 keV/60)	Target Lesion (TL)	24:88	0,968	0,931	1,000		0,957	0,916	0,999	
	1) Breast Tissue	24:80	0,559	0,437	0,680	<0.001	0,546	0,425	0,668	<0.001
	2) Muscle Tissue	24:88	0,468	0,345	0,590	<0.001	0,564	0,447	0,682	<0.001
	3) Aorta	24:88	0,299	0,153	0,444	<0.001	0,315	0,178	0,451	<0.001
Z effective	Target Lesion (TL)	24:88	0,977	0,942	1,000		0,975	0,943	1,000	
	1) Breast Tissue	24:80	0,541	0,423	0,659	<0.001	0,553	0,431	0,675	<0.001
	2) Muscle Tissue	24:88	0,465	0,346	0,584	<0.001	0,578	0,464	0,691	<0.001
	3) Aorta	24:88	0,331	0,186	0,476	<0.001	0,341	0,199	0,484	<0.001

3. Results

3.1. Examination and lesion characteristics

At site 1 117 spectral-CTs were carried out in female adults fulfilling the inclusion criteria (Fig. 1). 57 of the 117 CT-examinations (48.7%) were excluded due to normal breast findings, data acquisition in the arterial phase after i.v. contrast medium administration and/or a diagnostic follow-up < 2 years thus resulting in the inclusion of 66 lesions in 60 patients into the further evaluations. At site 2 259 spectral-CTs were referred by the Breast Center during the survey period. 115 of the 257 CT-examinations (44.8%) were excluded because they were part of an independent study and 94 CT-examinations were excluded due to normal breast findings in ultrasonography, mammography and breast MRI and/or a follow-up of <2 years in probably benign lesions.

The study group consisted of 98 patients with a mean age of 58.9 years (range 26–91 years) and 106 breast lesions (Table 1, Figs. 2–4). 96 of the 98 patients (98.0%) were female. Sixty patients (mean age 58.8, 26–91 years) with 66 breast lesions were recruited at site 1 and 38 patients (mean age 59.0, 4–84 years) with 40 breast lesions were included at site 2. Histological work-up was based on ultrasound-guided biopsies in the majority of cases (80 of 106; 75.5%). 81 of the 106 breast lesions (76.4%) had a malignant histology and 25 breast lesions (23.6%) were benign. The proportion of benign to malignant findings was 42:24 at site 1 and 39:1 at site 2, the distributional differences being due to the slightly differing inclusion and exclusion criteria used at both sites. 69 of the malignant breast lesions (85.2%) were classified as ≥ T1c (Table 1). With 63 of the 106 lesions examined (59.4%) invasive ductal carcinomas comprised the major part of histological diagnoses followed by invasive lobular carcinomas (9 of the 106 lesions, 8.0%).

3.2. Diagnostic evaluations

The areas under the ROC-curves (AUC) for the variables “density (HU)”, “iodine content (mg/ml)”, “VM curve-slope (HU 40 keV – HU 100 keV/60)” and the ratios “target lesion (TL) vs. breast tissue”, TL vs. muscle tissue” and “TL vs. aorta” of the variables “iodine content (mgl/ml)” and “Zeffective” (no unit) showed a high level of agreement between the independent assessments of both readers (Table 2, Figs. 5 and 6). The mean AUCs of the variables “iodine content” (reader 1: 0.974; reader 2: 0.976), of the variable “VM curve-slope” (0.968; 0.957) and the variable “Zeffective” (0.977; 0.975) measured in the target lesions showed statistically superior results compared to the AUCs of the variable “density” measured in the TL (0.929; 0.923) ($p < 0.001$) (Table 2).

The overlap of the AUCs measured in the TL and in the aorta (ratio “TL to aorta”) calculated for the variables “iodine content”, “VM curve-slope” and “Zeffective” was smaller than the overlaps of the AUCs calculated for the variables “iodine content”, “VM curve-slopes” and “Zeffective” measured in the TL vs. normal breast tissue and muscle (Table 2, Figs. 5 and 6), although the AUC-differences reached high statistical significance in all comparisons ($p < 0.001$).

The Youden indices (J) calculated for all variables and describing the empirical optimal cutpoint for the differentiation of benign vs. malignant findings as compared with histopathology as reference standard are given in Table 3. Referring to the variable “iodine content in the TL” a cutpoint of 0.88 mg/ml was calculated for reader 1 and a cutpoint of 0.73 mg/ml for reader 2 resulting in a sensitivity of 96.6% and a specificity of 91.7% for both readers, respectively. The variable “VM curve-slope” derived from the target lesions showed comparable results for both readers, the sensitivity ranging from 95.5% (reader 1) to 93.2% (reader 2) and a specificity of 91.7% (both readers) at an optimal calculated cutoff of 0.92 (reader 1) and 0.91 (reader 2). The iodine

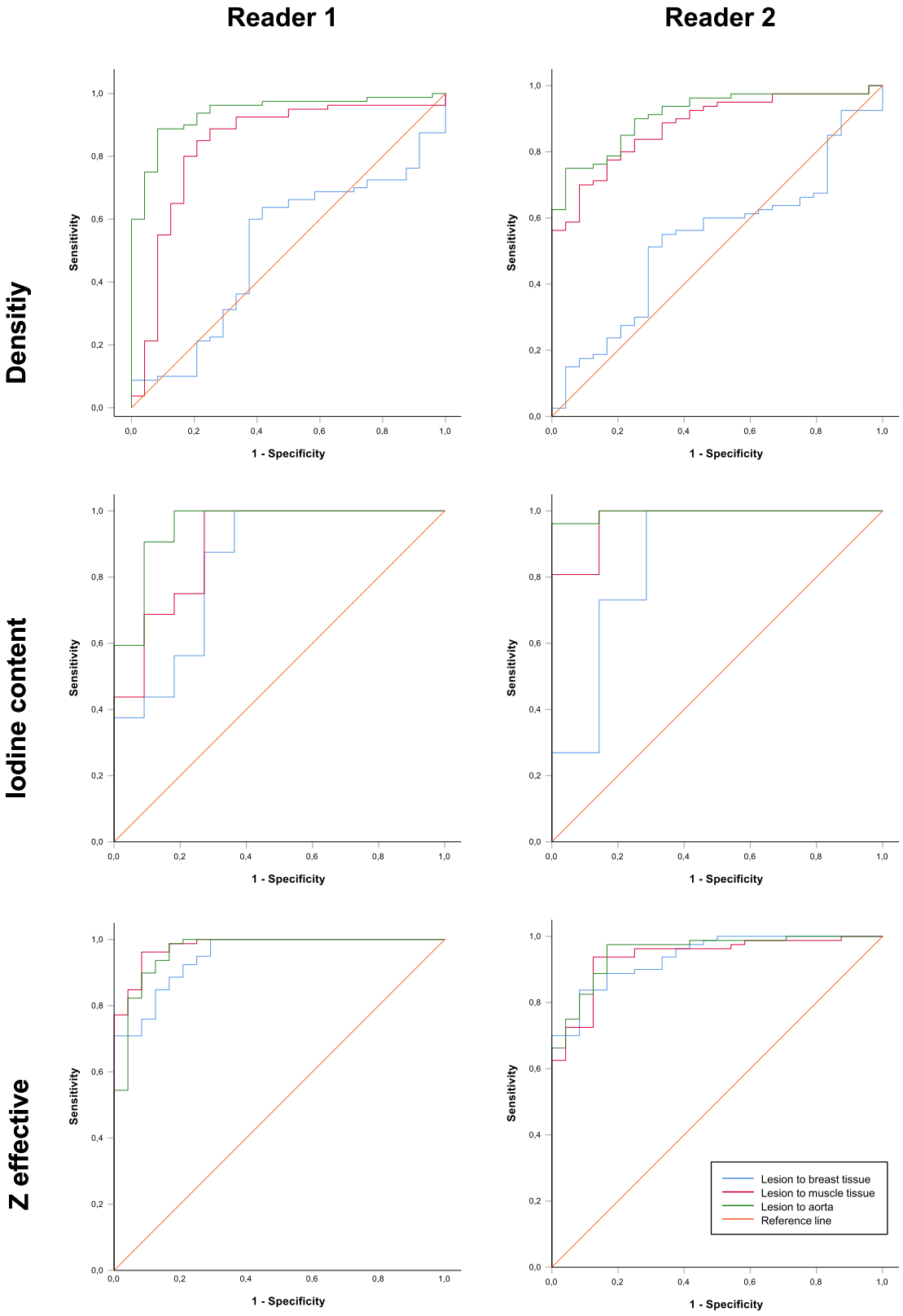

Fig. 5. The AUC curves for the parameters "density", "iodine content", and "Z effective" measured in the breast target lesions (TL) and normalized to those measured in healthy breast tissue, muscle tissue, and contrast enhanced blood in the aorta are separately given for reader 1 and reader 2. The best results were obtained when normalizing the mean iodine contents and the mean Z-effective values measured in the breast target lesions to contrast-enhanced blood in the aorta.

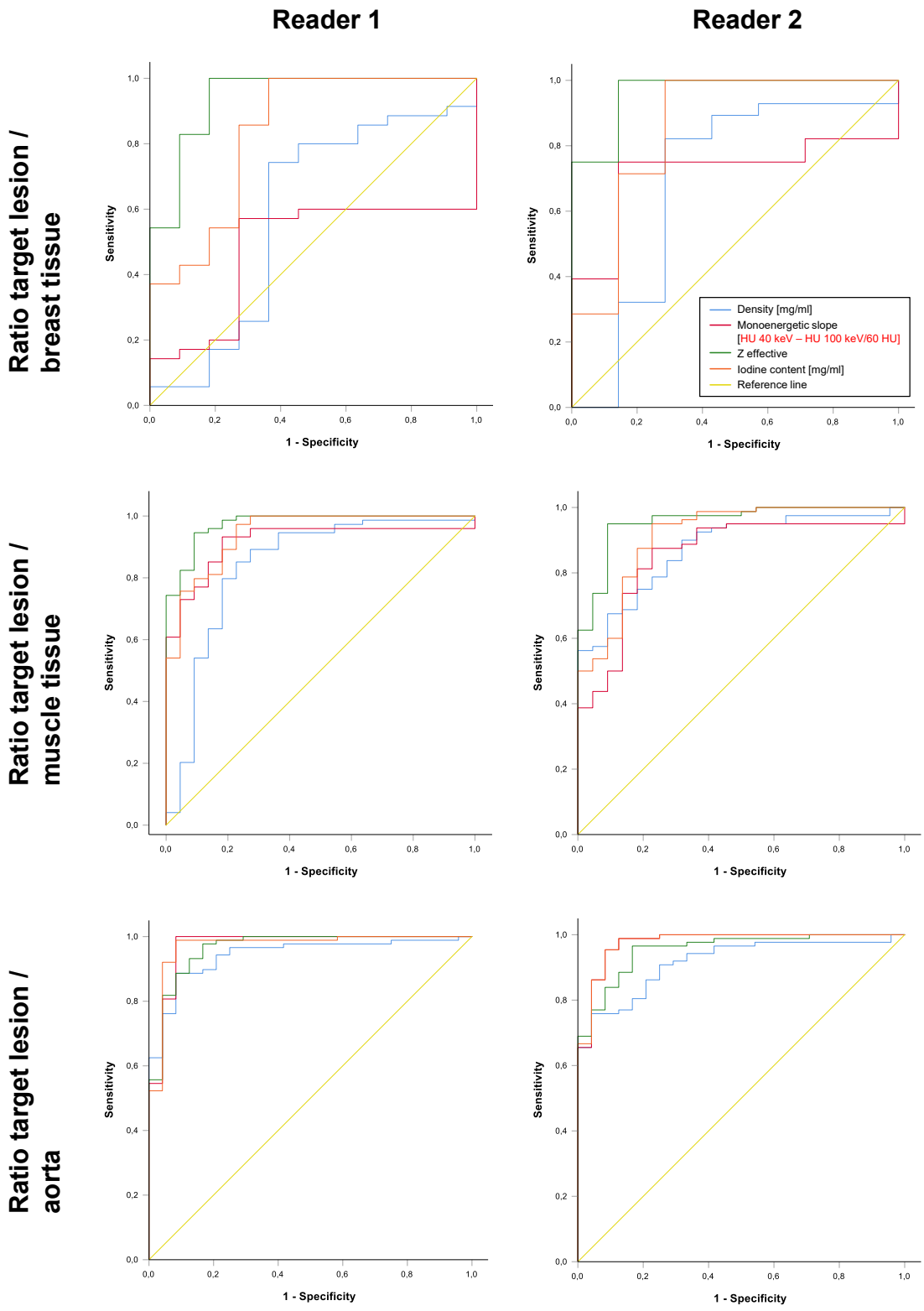

Fig. 6. The AUC curves of the ratios "TL to healthy breast tissue", "TL to muscle tissue" and "TL to aorta" were compared separately for the multiparametric spectral-CT parameters examined by reader 1 and reader 2. The best diagnostical results were achieved when normalizing the values measured in the TL to contrast-enhanced blood in the aorta using the parameters "iodine content", "monoenergetic slope" and "Z effective".

content measured in the TL showed best results when normalized vs. the iodine content in the aorta the Youden cut-point between both AUCs being calculated as 0.10 and 0.12 resulting in a sensitivity ranging from 95.5% to 98.9% and a specificity of 91.7% for both readers. With a Youden cutpoint of 7.73 for both readers, the variable "Zeffective" yielded comparably high sensitivities (reader 1: 96.6%, reader 2: 95.5%) with a specificity of 91.7% for both readers: 83.3%. The assessment of the variable "density" and the ratio "TL to aorta" yielded diagnostically inappropriate results with sensitivities ranging from 76.1% to 88.6% and specificities ranging from 91.7% to 95.8% at a cutpoint of 0.35 and

Table 3
Optimal cutpoints based on maximum Youden indices calculated from corresponding ROCs. The best diagnostic results are marked in bold print. TL = target lesion.

Variables	Calculations	Reader	Empirical optimal cutpoint	Sensitivity at cutpoint (%)	95% Confidence Interval (%)		Specificity at cutpoint (%)	95% Confidence Interval (%)	
					lower bound	upper bound		lower bound	upper bound
Iodine content (mg/ml)	TL	1	**0,88**	**96,60**	**90,40**	**99,30**	**91,70**	**73,00**	**99,00**
		2	**0,73**	**96,60**	**90,40**	**99,30**	**91,70**	**73,00**	**99,00**
Iodine content (mg/ml)	Ratio TL to breast tissue	1	2,37	100,00	95,90	100,00	29,20	12,60	51,10
		2	1,28	100,00	87,70	100,00	71,40	29,00	96,30
	Ratio TL to muscle tissue	1	1,67	97,70	92,00	99,70	70,80	48,90	87,40
		2	1,59	95,10	87,80	98,60	77,30	54,60	92,20
	Ratio TL to aorta	1	**0,10**	**98,90**	**93,80**	**100,00**	**91,70**	**73,00**	**99,00**
		2	**0,12**	**95,50**	**88,80**	**98,70**	**91,70**	**73,00**	**99,00**
Monoenergetic curve slope (HU 40 keV – HU 100 keV/60)	TL	1	**0,92**	**95,50**	**88,80**	**98,70**	**91,70**	**73,00**	**99,00**
		2	**0,91**	**93,20**	**85,70**	**97,50**	**91,70**	**73,00**	**99,00**
Density (HU)	Ratio TL to breast tissue	1	2,23	63,60	52,70	73,60	62,50	40,60	81,20
		2	1,76	51,20	39,80	62,60	70,80	48,90	87,40
	Ratio TL to muscle tissue	1	1,19	85,20	76,10	91,90	79,20	57,80	92,90
		2	1,23	69,30	58,60	78,70	91,70	73,00	99,00
	Ratio TL to aorta	1	0,35	88,60	80,10	94,40	91,70	73,00	99,00
		2	0,38	76,10	65,90	84,60	95,80	78,90	99,90
Z effective	TL	1	**7,73**	**96,60**	**90,40**	**99,30**	**91,70**	**73,00**	**99,00**
		2	**7,73**	**95,50**	**88,80**	**98,70**	**91,70**	**73,00**	**99,00**
Z effective	Ratio TL to breast tissue	1	1,11	85,20	76,10	91,90	87,50	67,60	97,30
		2	1,11	83,80	73,80	91,10	91,70	73,00	99,00
	Ratio TL to muscle tissue	1	1,04	95,50	88,80	98,70	91,70	73,00	99,00
		2	1,04	94,30	87,20	98,10	87,50	67,60	97,30
	Ratio TL to aorta	1	**0,77**	**97,70**	**92,00**	**99,70**	**83,30**	**62,60**	**95,30**
		2	**0,77**	**96,60**	**90,40**	**99,30**	**83,30**	**62,60**	**95,30**

0.38.

4. Discussion

In contrast to mammography, ultrasound and breast MRI, CT is not a primary method for evaluating breast masses due to its lower spatial resolution and high radiation dose [2,3,20–23]. However, solitary and multiple breast masses requiring further diagnostic evaluation are detected as incidental findings in up to 5.8% of all contrast-enhanced CT-examinations [2–5]. In such cases the evaluation of multiparametric information contained in spectral CT-datasets may help to distinguish clearly benign masses from etiologically ambiguous and malignant findings and thus may open the possibility of targeted senological clarification of the nature of breast lesions incidentially visualized in clinically indicated chest CT-examinations [21,24].

To our knowledge our study group is the largest to compare spectral-CT data of benign and malignant breast lesions and the only one persuing a multiparametric and quantitative approach including iodine-maps, virtual monoergetic-maps at 40 and 100 keV and Zeffective-maps. As main results we demonstrated that quantitative data derived from multiparametric maps of clinically indicated, contrast-enhanced, dual-energy CT-examinations of the chest allowing predictions about the biological value of solid breast lesions. Both of our readers agreed that iodine-maps demonstrated significantly higher iodine content in malignant masses compared to benign lesions with a cut-off of 0.73 mg/ml and 0.88 mg/ml, respectively (sensitivitiy 96.6%, specificity 91.7%, $p < 0.001$). The cut-off of the iodine content to distinguish benign from malignant breast masses found in our study was lower than the cut-off to discriminate invasive breast cancer and DCIS at the level of 1.7 mg/ml described by Volteranni et al. in their retrospective evaluation of 31 patients [18]. The higher cut-off in the study of Volteranni and colleagues is probably explained by the differences in scan delay after contrast injection between their study and our protocol (45–50 sec vs. 70 sec, respectively). In view of the fact that our study only comprised 3 DCIS the different definition of subgroups in both studies offers an unlikely explanation.

Furthermore, we were able to demonstrate based on 106 CT-examinations that the slope of the attenuation-curve of the VM-images, which depends on the iodine content in the healthy and diseased tissue, was significantly higher in malignant lesions with a cut-off value off 0.91 to 0.92, respectively (sensitivity 93.2% to 95.5%, specificity 91.7%).

In addition, we confirmed that visual perception of enhancing lesions were improved on VM-images at lower keV, an oberservation that was also true for the Zeffective-maps enabling the reliable detection of smaller lesions that could easily be overlooked on conventional CT. The VM-slopes calculated according to the formula "slope (k) = HU-value$_{40\ keV}$ − HU-value$_{100\ keV}$/60)" proved to be a stable predictor of malignancy with the optimal cutpoint in the breast target lesion being VM curve-slopes of 0.91 to 0.92, yielding a sensitivity of 93.2% to 95.5% and a specificity of 91.7%, respectively. The quantitative evaluation of the Zeffective-maps normalized to the contrast-enhanced blood in the aorta showed high sensitivities (96.6% to 97.7%), but a comparably low specificity of 83.3%, an observation that requires further clarification in future studies.

Our study had some limitations such as: There might be a sample bias, because the majority of the patients suffered from suspected or previously diagnosed invasive breast cancer and DCIS (81 examinations) and only a minority had benign breast lesions (25 examinations). The fact that predominantly larger focal lesions and tumors with classifications of ≥T1c were studied was due to the pilot character of the study, which aimed to verify the feasibility and appropriateness in principle of

a multiparametric evaluation approach for breast lesions visualized in clinically indicated spectral CT-examinations. Another limitation might be that we only included single-phase CT-scans performed in the portal-venous phase after i.v. contrast medium application. However, this procedure is in line with international guidelines [25]. Dynamic multi-phase CT-examinations carried out in order to visualize breast masses as performed by Okada et al. [16] are prohibited due to the high level of radiation exposure and its biological consequences the evaluation of dynamic signal intensity-to-time progressions thus remaining the domain of breast MRI in the long run.

In the future, studies with larger sample sizes focussing on smaller target lesions investigating whether the histologic grade of lesions could correlate with quantitatively measured iodine content could be useful. It could also be beneficial to evaluate whether demonstration of response to treatment could be possible in patients undergoing CT for surveillence purposes.

5. Conclusions

In conclusion, our preliminary results suggest that the multi-parameteric quantitative information contained in the iodine maps, VM-slope rates and Zeffective-values of dual spectral-CT-datasets may allow to estimate the benign or malignant nature of breast masses. Further prospective studies are warranted to validate these results. Although spectral-CT is not a method for dedicated breast examinations, patients with non-senological indications for chest CT-examinations could possibly benefit from a multiparametric evaluation approach of spectral CT-image datasets of breast lesions.

CRediT authorship contribution statement

Begüm Demirler Şimşir: Supervision, Investigation, Project administration, Writing - review & editing. **Kathrin Barbara Krug:** Supervision, Investigation, Project administration, Writing - review & editing. **Christina Burke:** Supervision, Investigation, Project administration, Writing - review & editing. **Martin Hellmich:** Supervision, Investigation, Project administration, Writing - review & editing. **David Maintz:** Supervision, Investigation, Project administration, Writing - review & editing. **Emmanuel Coche:** Supervision, Investigation, Project administration, Writing - review & editing.

Declaration of Competing Interest

The authors declare that they have no known competing financial interests or personal relationships that could have appeared to influence the work reported in this paper.

References

[1] K.B. Krug, C. Houbois, O. Grinstein, et al., Focal Breast Lesions in Clinical CT-examinations of the Chest: A Retrospective Analysis, Rofo. 189 (2017) 977–989, https://doi.org/10.1055/s-0043-112749.

[2] M. Dietzel, P.T.A. Blatzer, How to use the Kaiser score as a clinical decision rule for diagnosis in multiparametric breast MRI: a pictorial essay, Insights Imag. http://dx.doi.10.1007/s13244-018-0611-8.

[3] M. Inoue, T. Sano, R. Watai, et al., Dynamic multidetector CT of breast tumors: diagnostic features and comparison with conventional techniques, AJR Am. J. Roentgenol. 181 (2003) 679–686, https://doi.org/10.2214/ajr.181.3.1810679. PMID: 12933459.

[4] W.C. Lin, H.H. Hsu, C.S. Li, et al. Incidentally detected enhancing breast lesions on chest computed tomography. Korean J. Radiol.12 (2011) 44–51. http://dx.doi.10.3348/kjr.2011.12.1.44 (Epub 2011 Jan 3. PMID: 21228939; PMCID: PMC3017883).

[5] P. Moyle, L. Sonoda, P. Britton, R. Sinnatamby, Incidental breast lesions detected on CT: what is their significance? Br. J. Radiol. 83 (2010) 233–240. http://dx.doi.10.1259/bjr/58729988 (Epub 2009 Jun 22. PMID: 19546179; PMCID: PMC3473543).

[6] M.G. Harish, S.D. Konda, H. MacMahon, G.M. Newstead, Breast lesions incidentally detected with CT: what the general radiologist needs to know, Radiographics. 27 (Suppl 1) (2007) S37–S51, https://doi.org/10.1148/rg.27si075510. PMID: 18180233.

[7] E.J. Chae, J.W. Song, J.B. Seo, B. Krauss, Y.M. Jang, K.S. Song, Clinical utility of dual-energy CT in the evaluation of solitary pulmonary nodules: initial experience, Radiology 249 (2008) 671–681, https://doi.org/10.1148/radiol.2492071956. Epub 2008 Sep 16 PMID: 18796658.

[8] C.N. De Cecco, A. Darnell, M. Rengo, et al., Dual-energy CT: oncologic applications, AJR Am. J. Roentgenol. 199 (Suppl. 5) (2012) S98–S105, https://doi.org/10.2214/AJR.12.9207. PMID: 23097174.

[9] S. Lennartz, M. Le Blanc, D. Zopfs, N. Große Hokamp, N. Abdullayev, K.R. Laukamp, S. Haneder, J. Borggrefe, D. Maintz, T. Persigehl, Dual-Energy CT-derived Iodine Maps: Use in Assessing Pleural Carcinomatosis, Radiology 290 (2019) 796–804. http://dx.doi.10.1148/radiol.2018181567 (Epub 2019 Jan 15. PMID: 30644812).

[10] D. Zopfs, N. Große Hokamp, R. Reimer, G. Bratke, D. Maintz, C. Bruns, C. Mallmann, T. Persigehl, S. Haneder, S. Lennartz, Value of spectral detector CT for pretherapeutic, locoregional assessment of esophageal cancer, Eur. J. Radiol. 134 (2020) 109423, https://doi.org/10.1016/j.ejrad.2020.109423. Online ahead of print.PMID: 33302024.

[11] N. Große Hokamp, D. Maintz, N. Shapira, H. Chang, P.B. Noël, Technical background of a novel detector-based approach to dual-energy computed tomography, Diagn. Interv. Radiol. 26 (1) (2020 Jan) 68–71, https://doi.org/10.5152/dir.2019.19136. PMID: 31904573.

[12] T.R. Johnson, Dual-energy CT: general principles, AJR Am. J. Roentgenol. 199 (Suppl. 5) (2012) S3–S8, https://doi.org/10.2214/AJR.12.9116. PMID: 23097165.

[13] C.H. McCollough, S. Leng, L. Yu, J.G. Fletcher, Dual- and Multi-Energy CT: Principles, Technical Approaches, and Clinical Applications, Radiology 276 (2015) 637–653, https://doi.org/10.1148/radiol.2015142631. PMID: 26302388; PMCID: PMC4557396.

[14] N. Rassouli, M. Etesami, A. Dhanantwari, P. Rajiah, Detector-based spectral-CT with a novel dual-layer technology: principles and applications, Insigh. Imag. 8 (2017) 589–598, https://doi.org/10.1007/s13244-017-0571-4. Epub 2017 Oct 6. PMID: 28986761; PMCID: PMC5707218.

[15] Y. Okamura, N. Yoshizawa, M. Yamaguchi, I. Kashiwakura, Application of dual-energy computed tomography for breast cancer diagnosis, Int. J. Med. Phys. Clin. Eng. Radiat. Oncol. 5 (2016) 288–297, https://doi.org/10.4236/ijmpcero.2016.54029.

[16] K. Okada, M. Matsuda, T. Tsuda, et al., Dual-energy computed tomography for evaluation of breast cancer: value of virtual monoenergetic images reconstructed with a noise-reduced monoenergetic reconstruction algorithm, Jpn. J. Radiol. 38 (2020) 154–164, https://doi.org/10.1007/s11604-019-00897-1. Epub 2019 Nov 4 PMID: 31686294.

[17] Y. Metin, N.O. Metin, O. Özdemir, F. Taşçı, S. Kul, The role of low keV virtual monochromatic imaging in increasing the conspicuity of primary breast cancer in dual-energy spectral thoracic CT-examination for staging purposes, Acta Radiologica. 61 (2020) 168–174, https://doi.org/10.1177/0284185119858040.

[18] L. Volterrani, F. Gentili, A. Fausto, et al., Dual-energy CT for locoregional staging of breast cancer: preliminary results, AJR Am. J. Roentgenol. 214 (2020) 707–714, https://doi.org/10.2214/AJR.18.20953.

[19] W.J. Youden, Index for rating diagnostic tests, Cancer 3 (1) (1950) 32–35, https://doi.org/10.1002/1097-0142(1950)3:1<32::aid-cncr2820030106>3.0.co;2-3.

[20] C.H. Lee, D.D. Dershaw, D. Kopans, et al., Breast cancer screening with imaging: recommendations from the Society of Breast Imaging and the ACR on the use of mammography, breast MRI, breast ultrasound, and other technologies for the detection of clinically occult breast cancer, J. Am. Coll. Radiol. 7 (2010) 18–27, https://doi.org/10.1016/j.jacr.2009.09.022. PMID: 20129267.

[21] A. Milulescu, L. Di Marino, N. Peradze, A. Toesca, Management of Multifocal-Multicentric Breast Cancer: Current Perspective, Chirurgia (Bucur). 112 (2017) 12–17, https://doi.org/10.21614/chirurgia.112.1.12. PMID: 28266287.

[22] American College of Radiology (ACR), American College of Radiology ACR Appropriateness Criteria® Breast Cancer Screening, Breast Cancer Screening (acr.org).

[23] C. Robertson, S.K. Ragupathy, C. Boachie, et al., Mammographic Surveillance Health Technology Assessment Group. Surveillance mammography for detecting ipsilateral breast tumour recurrence and metachronous contralateral breast cancer: a systematic review, Eur. Radiol. 21 (2011) 2484–2491, https://doi.org/10.1007/s00330-011-2226-z. Epub 2011 Aug 11. PMID: 21833567; PMCID: PMC3217137.

[24] A. Neri, D. Marrelli, T. Megha, et al., Clinical significance of multifocal and multicentric breast cancers and choice of surgical treatment: a retrospective study on a series of 1158 cases, BMC Surg. 15 (2015) 1, https://doi.org/10.1186/1471-2482-15-1. PMID: 25586679; PMCID: PMC4324662.

[25] American College of Radiology (ACR), ACR Appropriateness Criteria®, Imaging of Mediastinal Masses. https://acsearch.acr.org/docs/3157912/Narrative/.